# Camera Guided Real-Time Laser Ranging for Multi-UAV Distance Measurement

**Denis Ojdanić**[1,*], **Benjamin Gräf**[1], **Andreas Sinn**[1], **Han Woong Yoo**[1], **and Georg Schitter**[1]

[1] *The authors are with the Automation and Control Institute (ACIN), Technische Universität Wien, 1040 Vienna*
[*] *Corresponding author: ojdanic@acin.tuwien.ac.at*

*Compiled October 4, 2022*

**This paper presents the design and implementation of a scalable laser ranger finder (LRF) based prototype system, which enables distance measurement and precise localization of multiple UAVs in real-time. The system consists of a telescope and camera as the image acquisition components, supplemented by an LRF and a fast steering mirror (FSM) to obtain the distance measurement. By combining the optical path of the camera and the LRF through a dichroic mirror, the LRF is accurately aligned by the FSM based on the angular position of a UAV within the camera field of view. The implemented prototype successfully demonstrates distance measurements of up to 4 UAVs with a bandwidth of 14 Hz per object.** 

http://dx.doi.org/10.1364/ao.XX.XXXXXX

## 1. INTRODUCTION

The popularity of unmanned aerial vehicles (UAVs) has grown exponentially over the past several years [1]. Unfortunately, the commercial success is accompanied by a simultaneous growth of incidents in safety critical areas. Airports, for instance, are highly vulnerable to undetected UAVs as an occurrence around the Los Angeles International Airport shows, where a commercial jet almost collided with a UAV during approach [2]. In 2015 multiple UAVs were sighted in the proximity of several nuclear power plants in France [3] and studies on the threat posed by UAVs to the mentioned facilities highlight the necessity of deployment of appropriate technological solutions for detection and neutralization [4]. Besides the apparent threat to critical infrastructure, UAVs are versatile tools for the smuggling of goods across state boarders or in and out of prisons [5, 6]. Furthermore, recent developments in the control of multiple drones as swarms may revolutionize future threat scenarios as for example multiple UAVs flying in close formation increase the chance of reaching the desired destination through redundancy [7, 8]. Given the rising number of UAVs sold every year paired with the alarming amount of reported incidents, development and installation of UAV reconnaissance systems for precise UAV localization are paramount to prepare appropriate defensive countermeasures.

Various UAV detection and distance measurement methods have been researched extensively over the past decade. Radio frequency detection for example exploits the communication link between operator and the UAV to localize targets over distances of 5 km with accuracies of about 5° [9, 10]. Similar UAV localization accuracies over distances up to 600 m are achievable by the usage of acoustic microphone arrays recording the ambient sound and applying suitable signal analysis methods [11, 12]. While being able to detect multiple objects simultaneously, the achieved accuracies do not allow precise localization needed for directed countermeasures.
Electro-optical systems use cameras to capture images and reconnaissance of UAVs is performed by advanced computer vision algorithms [13] with operational ranges for typical systems going up to

2 km [14]. Estimations through a monocular vision approach are possible by applying for example pose estimation using a skeleton model of the UAV [15] or using deep neural networks [16], however the localization accuracy suffers greatly for long ranges [17]. Stereo vision provides better results for distance measurements and is used for autonomous driving, robotics and 3D building mapping [18]. For accurate measurements over long distances, the two cameras need to be displaced further away, which makes the system more complex.

RADAR actively sends out a signal as radio wave and acquires the distance to an object by measuring the signal reflected by the target. It has been shown that RADAR is capable of detecting even small objects like consumer UAVs over distances of several kilometres [19]. Whereas detection is possible, object tracking is not reliable as it heavily depends on the objects radar cross section and the surrounding terrain [14].

Methods based on the time of flight (ToF) principle are emitting an electro-magnetic wave and measuring the reflected signal to infer the distance [20]. LiDAR, is one example for a ToF measurement, which is often used for autonomous vehicular applications [21] and has been applied to measure the distance to UAVs [22, 23]. Flashing LiDAR uses a diverging laser, which illuminates the whole field of view (FoV) and the reflected signal is measured by a matrix of photodiodes [24]. Flashing LiDAR cameras exist with operational ranges of up to 1000 m, nevertheless, the achievable resolution is low and does not allow to detect small objects like UAVs over long distances [25]. Rotating and scanning LiDAR are modifications to achieve longer distances by using collimated laser beams with little divergence and sequentially measuring the field of view (FoV) [26]. Studies have been conducted using rotating LiDAR to detect UAVs [22], concluding that the resolution depends on the number of vertical sensors in the receiver array. Scanning LiDAR extends the operational range to a few kilometres [27, 28], however, sequentially measuring a large FoV is time consuming and not suited to localize small and fast moving objects. The combination of ranging with optical imaging systems has been studied extensively to generate terrain maps with topography information [29] and for atmospheric remote sensing [30, 31]. To measure the distance to UAVs, bi-axial systems have been proposed consisting of a dome equipped with a camera and laser ranger finder (LRF)s aiming at the center of the camera FoV [32]. To obtain a measurement, the dome has to align the object within the center of the camera FoV, which limits the achievable bandwidth of the system making a real-time multi-object distance measurement infeasible. Generally, sensor fusion is applied to build holistic UAV detection and localization systems combining the strengths of various approaches, for example RADAR or acoustics to detect an object and electro-optics for the visual confirmation. [33–35] Nonetheless, an accurate long distance localization of multiple objects in real-time is still challenging with the described methods.

The contribution of this paper is the integration of a steerable LRF with a telescope system, which enables multi-UAV distance measurement by aiming the LRF with an FSM towards a UAV position extracted within a camera frame. The laser transmitter and camera optical path are combined by a dichroic mirror, merging the visual and the infrared light, allowing real-time alignment of the LRF. The article is organized as follows. Section 2 describes the proposed concept and implemented system. In Section 3 the required laser power is analysed and in Section 4 the distance measurement strategy is discussed in more detail. Finally, the experiments and results are shown in Section 5 followed by concluding remarks in Section 6.

## 2. SYSTEM DESCRIPTION

The main components of the system are the camera and telescope for image acquisition [36], the LRF for distance measurements and further optical elements for the alignment of visual and laser light paths. The key advantage of the proposed concept is the possibility to obtain the distance to an object by a single LRF measurement, as the laser beam is overlapping with the optical path of the visual light as indicated by the violet lines in Fig. 1a. The combination of the two light beams is facilitated by a dichroic mirror, which is transparent for wavelengths of the visible spectrum and reflective for infrared light. Objects, like UAVs, are extracted from camera frames by the usage of computer vision algorithms and based on the position within an image, the LRF beam direction is adjusted by a fast steering mirror (FSM). By applying this idea, no scanning of the FoV is required

Post-print version of the article: D. Ojdanic, B. Gräf, A. Sinn, H. W. Yoo, and G. Schitter, "Camera Guided Real-Time Laser Ranging for Multi-UAV Distance Measurement," *Applied Optics*, vol. 61, 2022. DOI: 10.1364/AO.470361

Post-print version (generated on 09.11.2022)
**This and other publications are available at:**
http://www.acin.tuwien.ac.at/publikationen/ams/



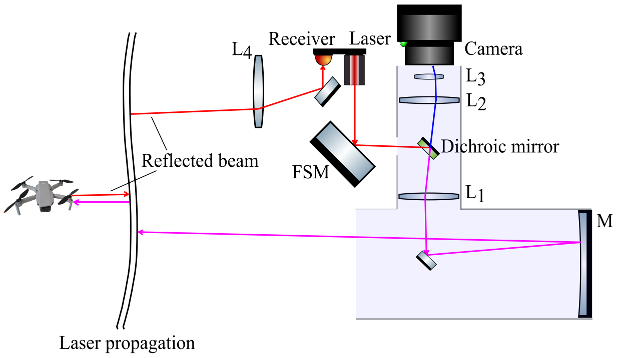


**(a)** Schematic overview of the optical setup.

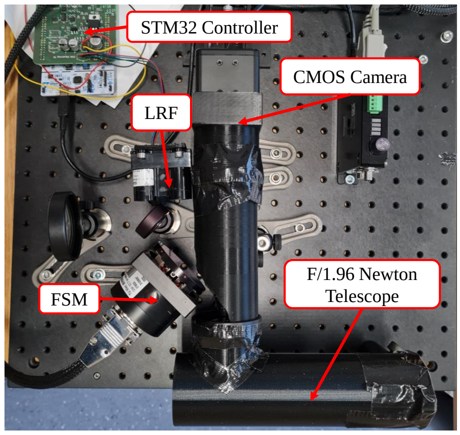


**(b)** Illustration of the implemented system.

**Fig. 1.** Overview of the optical setup consisting of a custom built Newtonian telescope and a commercially available CMOS camera for image acquisition. (a) Schematic overview: The LRF LiDAR-Lite v3 is used to measure the distance to a UAV and the LRF transmit beam is steered by an OIM102 FSM. The optical paths of the visual (blue) and infrared light (red) are merged by a dichroic mirror (violet). Table 1 shows details about the used components. (b) Image of the implemented small scale prototype: A STM32 Nucleo-64 controller board is responsible for interfacing and controlling the LRF and the FSM.

to find objects and the distance is obtained by a single LRF measurement. Finally, the proposed optical setup can be attached to a mount allowing pan and tilt motion to observe a 360° area, whereas simultaneous distance measurement is possible for objects within the field of view of the telescope [36]. The FSM based laser steering system allows fast acquisition and hence, distance measurements as soon as the object is within the field of view of the camera and detected by the computer vision algorithm. Rigidly mounted LRFs require a centering procedure of the telescope to enable the position measurement [32], which may be a time consuming procedure in case of multiple UAVs. Furthermore, the mount may be used to pan and tilt to another UAV or group of UAVs of interest.

**Table 1.** Sizes and focal lengths of the optical lenses and mirrors used in the setup.

| Name | Diameter | Focal length |
|---|---|---|
| Dichroic mirror | 12.7 mm | |
| Secondary mirror | 12.7 mm | |
| FSM | 50.8 mm | |
| $M$ | 50.8 mm | 100 mm |
| $L_1$ | 50.8 mm | 100 mm |
| $L_2$ | 50.8 mm | 100 mm |
| $L_3$ | 23 mm | 50 mm |
| $L_4$ | 50.8 mm | 125 mm |

### A. System Components

To demonstrate the concept, a small scale prototype system is implemented as shown in Fig. 1b. The LiDAR-Lite v3 (Garmin, USA) is selected as an LRF, which has a maximum measurement range of 40 m and is operated at an update rate of 117 Hz. The laser beam has a wavelength of 905 nm at a beam divergence of 8 mrad. The peak power of the LRF is 1.3 W with a pulse duration of 500 ns. The communication to the LRF is established via an inter-integrated circuit ($I^2C$) interface. For an accurate and quick laser alignment the OIM102 (Optics In Motion, USA) FSM is responsible, which has an mechanical range of $\pm$ 1.5° and a $-3$ dB bandwidth of 750 Hz for reference signals of 1.5 millidegrees. To control the FSM and the LRF, a custom build extension board is designed for a STM32 Nucleo-64 (MB1136) board (STMicroelectronics, Switzerland).

Post-print version of the article: D. Ojdanic, B. Gräf, A. Sinn, H. W. Yoo, and G. Schitter, "Camera Guided Real-Time Laser Ranging for Multi-UAV Distance Measurement," *Applied Optics*, vol. 61, 2022. DOI: 10.1364/AO.470361

A CMOS camera (Ailipu Technology Inc., China) is used to capture images with a sensor width of 5.76 mm and height of 4 mm. The camera provides 24 frames per second (FPS) and is run with a resolution of 640 x 480 pixels. To focus the light on the camera sensor a Newtonian telescope with a focal length of 100 mm and a 2 inch aperture size is built. The focal ratio of f/1.96 is used as it allows a wide FoV for short ranges complementary to the achieved distances by the LRF. Finally, the combination of infrared and visual light is facilitated through a partly reflective and partly transmissive dichroic mirror. For the setup the DMSP805T (Thorlabs Inc, Germany) half inch short short-pass dichronic mirror is selected, which has a cut-off wavelength of 805 nm. Below the cutoff wavelength the mirror is transmissive and wavelengths above this threshold are reflected. The system is easily scalable to longer operational distances by selecting a more powerful long range LRF and an adequate telescope.

## 3. SYSTEM ANALYSIS

In this section, the influence of an offset between the optical paths between the camera and LRF are discussed justifying the proposed concept. Additionally, a model is presented for required laser power and the achievable measurement distances for the prototype system.

### A. Laser to Camera Offset

For the design of a system, which optically detects and subsequently measures the distance to a UAV using an LRF, the offset $d$ between the path of the camera light and the laser is crucial. A simple solution is by placing the LRF close to the optical aperture [32] as depicted in Fig. 2a. The minimal distance $R_m$ for which an object with a diameter of $w$ is fully illuminated by a laser beam is given by

$$R_m = \frac{d + \frac{w}{2}}{tan(\theta_t)}, \quad (1)$$

where $d$ is the LRF to camera offset of 0.1 m. Using the LiDAR-Lite v3 as an LRF of the small scale system with a beam divergence of 8 mrad, an object with a diagonal dimension of 0.05 m, corresponding to the surface area of the body of a front facing DJI Mini 2 excluding the rotors, will be fully illuminated in a distance of 15.6 m. Below this distance, the object is illuminated only partly, resulting in less

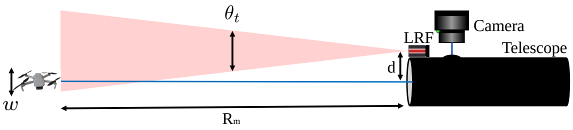


**(a)** Offset $d$ between optical paths of camera and LRF.

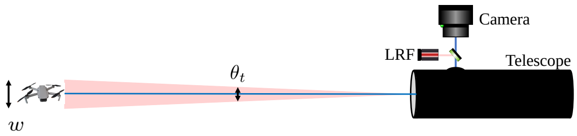


**(b)** No offset between optical paths of camera and LRF.

**Fig. 2.** The optical path of the camera and the LRF are separated by a distance $d$ (a). An object of size $w$ is fully illuminated in distances greater than $R_m$. Below this distance, a correct measurement is not guaranteed, as most of the laser beam is missing the target. Reducing the beam divergence $\theta_t$ increases the distance $R_m$. To overcome these problems, the optical path of the camera and the LRF are merged (b). The distance to the UAV can be obtained by a single LRF measurement. Reducing the beam divergence $\theta_t$ has no negative effect on the operational range of the system and can even increase the measurement distance for small objects.

reflected laser power, which degrades the measurement quality. In a distance below 9.4 m the object is completely missed. For an upscaled system covering long measurement distances, similarly the camera to laser offset leads to a potential target miss. To enable measurements over the whole range, the epipolar line, being the blue line in Fig. 2a, has to be scanned at a cost of reduced system bandwidth, as multiple LRF measurements are necessary to find the object in the first place. Another approach is to combine the two optical paths of the laser beam and the camera as presented in Section 2 and in Fig. 2b, which automatically aligns the laser with the camera image. While the optical system of Fig. 2b is more complex and leads to an increased optical loss, the configuration allows high bandwidth, which is indefensible for real-time distance measurement.

### B. Laser Power

A crucial design parameter for the ToF principle is the required laser peak power, as it directly influences the light intensity hitting the object and therefore forms the basis of the reflected signal. Using the typical rangefinder relation the received laser power

Post-print version of the article: D. Ojdanic, B. Gräf, A. Sinn, H. W. Yoo, and G. Schitter, “Camera Guided Real-Time Laser Ranging for Multi-UAV Distance Measurement,” *Applied Optics*, vol. 61, 2022. DOI: 10.1364/AO.470361

**Table 2.** Overview of the parameters for Eq. (2).

| Symbol | Quantity |
|---|---|
| $\tau_a$ | Atmospheric transmission loss factor |
| $\tau_o$ | Optical transmission factor |
| $D_R$ | Diameter of receiver optics |
| $\rho_t$ | Target reflectivity |
| $d_A$ | Effective surface area of the target |
| $R$ | Distance between LRF and target |
| $\theta_R$ | Target surface angular dispersion |
| $\theta_t$ | Laser beam divergence |

$P_{det}$ can be determined by

$$P_{det} = \frac{\tau_a^2 \tau_o D_R^2 \rho_t d_A}{R^2 \theta_R (\theta_t R)^2} P_{peak}, \tag{2}$$

with the transmitted peak laser power $P_{peak}$ and the remaining parameters from Table 2 [37]. The atmospheric transmission loss factor $\tau_a$ is given by

$$\tau_a = e^{-\gamma R}, \tag{3}$$

with $\gamma$ being the atmospheric extinction coefficient [38]. For the presented calculation $\gamma$ is set to $0.096\,\mathrm{km}^{-1}$, which resembles excellent atmospheric conditions [38]. Using Eq. (2) together with the specifications in the datasheet of the LiDAR Lite v3, the maximally achievable measurement distance for various target distances and sizes can be inferred for the optical setup in Fig. 1b. As the LRF is intended to be incorporated into a system consisting of various optical elements as seen in Fig. 1a, a loss factor for the optical components $\tau_o$ and an increased receiver aperture size of 50.8 mm are considered. Fig. 3 shows the necessary peak power to measure the distance to different target sizes. Due to the noise of most detectors of LiDARs, the maximal detection distance in reality is influenced by environmental conditions such as ambient light and temperature [39]. The influence of the effective target surface area $d_A$ is visible in Fig. 3 through the bend in the laser transmitter power curves. Above this bend, the required laser peak power increases more rapidly with the distance, as the laser beam cross section is larger than the target, which results in a loss of energy as part of

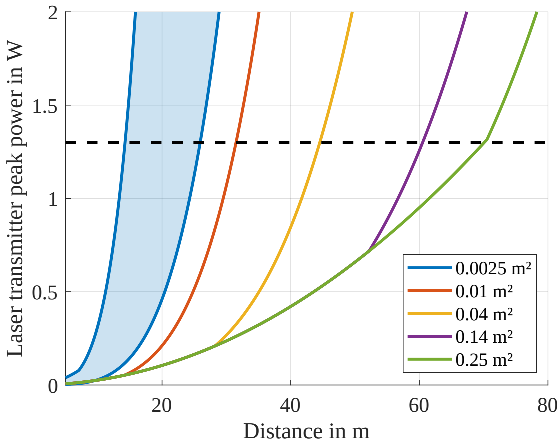


**Fig. 3.** The effect of different target sizes on the achievable measurement distance for the LRF of the small scale prototype system for a challenging target reflectivity of 30 % and an receiver aperture size of 50.8 mm. The dashed black line represents the peak laser power of 1.3 W according the datasheet. Additionally, the impact of the target material reflectance $\rho$ is depicted in blue for an object of 0.05 m x 0.05 m and the reflectance ranging from 0.05 % to 0.55 %.

the laser light is not reflected by the target. In practice, the laser power cannot be simply increased for a long range detection considering saturation with high gain detectors at short distances and laser safety for human eye and skin [39, 40]. Therefore, keeping the laser beam cross section smaller than the effective surface area maximizes the amount of reflected laser light by the target and thus the achievable measurement distances. The dashed black line represents the LRF peak power of 1.3 W resulting in a theoretical maximum measurement distance of roughly 70 m for a target size of $0.25\,\mathrm{m}^2$.

An important property for the analysis is the target reflectivity, as it has a great impact on the system performance. Depending on the type and colour of the plastic of the UAV a wide range of reflectivity $\rho_t$ is applicable [41, 42]. For the presented model, a conservative reflectivity in the lower range of 5 % to 55 % is selected, as the properties of an intruding UAV is not known a priori. In Fig. 3 the shaded blue area shows an achievable measurement range between 14 m to 26 m for an object size of 0.05 m x 0.05 m for the investigated reflectivity range. As stated in Section 2, the small scale prototype system is scalable to longer operational ranges by selecting a stronger laser and a lower beam divergence.

## 4. DISTANCE MEASUREMENT STRATEGY

The position of a UAV in a video frame is extracted by computer vision algorithms. As the goal is a proof of concept of the proposed design, the Kernelized Correlation Filter (KCF) tracker provided by OpenCV [43] is used, which is initialized manually to track a certain object. Based on the position provided by the algorithm, the LRF is accurately aligned by the FSM to obtain the distance to the object. Combining the object position within a frame with the measured distance, an exact horizontal localization of the objects relative position to the setup is calculated by

$$x = R \cdot tan(\alpha)\frac{f_x}{f_w}, \tag{4}$$

where $\alpha$ represents half of the angular horizontal FoV, $R$ the distance to the object, $f_x$ the offset of the object from the frame center in pixels in vertical direction and $f_w$ the frame width in pixels. A similar calculation returns the $y$ coordinate or the vertical position of the object replacing $f_x$ with the offset in vertical direction $f_y$. The center of the coordinate system is situated at the telescope entry and by knowing the telescope position, the object can be localized precisely. In addition to knowing the precise object location, the object size can be determined based on the distance and the number of pixels covered by the object.

The benefit of the proposed concept is the possibility to align the laser to the UAV without the need of performing a scan with the laser to initially find the UAV. Nevertheless, as shown in the Section 5, some measurements might still miss the UAV due to non perfect bounding box localization by the computer vision algorithm and due to the complex shape of UAVs. Increasing the beam divergence, similar to flashing LiDAR, is an approach to deal with this issue, but this increases the required laser power according to Eq. (2) and is therefore not feasible. Another solution, at the expense of system bandwidth, is to perform a local scan of the area suggested by the bounding box of the computer vision algorithm using the FSM. The latter approach is selected, where multiple laser distance measurements are conducted inside the bounding box using a raster scanning trajectory. The obtained data points are clustered via the k-means clustering algorithm to extract the object in the foreground. The average distance of the foreground cluster is taken as the measured UAV distance.

Additionally, the setup allows to measure the distance to multiple objects in real-time by realigning the laser beam direction through tip and tilt motions of the FSM. When measuring the distance to an increasing number of objects, the system bandwidth, meaning the distance measurements performed per UAV, is reduced. After acquiring a frame and subsequently the positions through the computer vision algorithm, the bandwidth is comprised of the sequential FSM alignment and the LRF measurement. To improve the system performance the path between UAVs travelled by the FSM is optimized to reduce the movement of the mirror. To achieve this optimization, a brute force approach is chosen to calculate the shortest path between multiple UAVs.

## 5. EXPERIMENTS AND RESULTS

For the experimental analysis, indoor tests at room temperature are performed using targets of different sizes and materials to quantify the distance measurement capabilities of the small scale setup. Furthermore, experiments with UAVs are conducted to test the effect of small and complex shaped objects on achievable distances. Finally, an evaluation of the multi-object measurement performance is conducted.

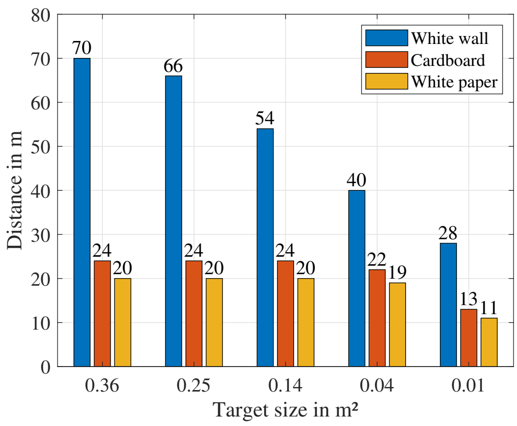


**Fig. 4.** Measured maximum distances for different target sizes and materials using the small scale prototype system.

Post-print version of the article: D. Ojdanic, B. Gräf, A. Sinn, H. W. Yoo, and G. Schitter, “Camera Guided Real-Time Laser Ranging for Multi-UAV Distance Measurement,” *Applied Optics*, vol. 61, 2022. DOI: 10.1364/AO.470361

### A. Target size

The first part of the experiments examines the achievable distances of the small scale prototype system for varying target sizes, distances and materials to validate the presented model in Section 3. The evaluation setup is inspired by the LAS test station by Inframet, where the distance to targets of different sizes and reflectivity is measured [44]. In contrast to the proposed procedure, two smaller targets with the dimensions of 0.2 m x 0.2 m and 0.1 m x 0.1 m are added, which correspond to smaller UAV sizes like consumer drones. To obtain the maximum measurable distance, a target is used, which is larger than the beam diameter resulting in a maximum operation range of 70 m. The increase in achievable distance compared to the information provided in the datasheet is largely contributed to the added receiver optics $L_4$. The results for different target sizes and materials are presented in Fig. 4 and the impact of the decreasing object surface is evident for the white wall, as long distances are achievable due to its strong reflectivity. The laser beam area increases with the distance and as the target size is surpassed, less power is reflected and more transmit power is needed to further increase the operational range, which manifests itself as the steep increase in the required laser peak power curves visible in Fig. 3. To mitigate this problem, the laser beam divergence can be further reduced. Comparing the measurement results in Fig. 4 to the model in Fig. 3 the model shows slightly longer expected distances for example 70 m for a target size of 0.25 m$^2$ compared to the measured 66 m. To evaluate small and complex shaped objects, the maximal measurement distance to a DJI Mini 2 is measured at 15 m, which fits within the lower range of the expected distances as presented in Fig. 3 in the shaded blue area. The experiments show that the estimation of achievable distances according to the model in (2) corresponds to the measured results.

### B. Multi-object measurement

In the following an analysis of the system bandwidth, which corresponds to the achievable frame rate, is given. The camera represents a fundamental limit achieving 24 FPS. Processing of a frame by computer vision algorithms to extract the object location adds delay, however, for multi target tracking parallel approaches can reduce the inference time. After obtaining the object position within a camera frame, the multi-object distance measurement is executed sequentially. The main components limiting the bandwidth are the FSM and the LRF. As stated in Section 2 the LRF has a bandwidth of 117 Hz or 8.5 ms between each measurement. The FSM has a −3 dB bandwidth of 750 Hz for small drive angles of a few millidegrees. To support coverage of the complete camera FoV, the mirror has to be operated in the full angular range of $\pm$ 1.5°, which reduces the bandwidth to 154 Hz or a settling time of 6.5 ms. To obtain the settling time, a step response is applied as an input signal to the FSM, which results in a 3° mirror step. The time between the application of the input signal and the first intersection with the step response is defined as settling time, as the FSM controller is tuned to have a small overshoot. The time of communication components responsible for sending position commands to the FSM is neglected as it is in the range of microseconds.

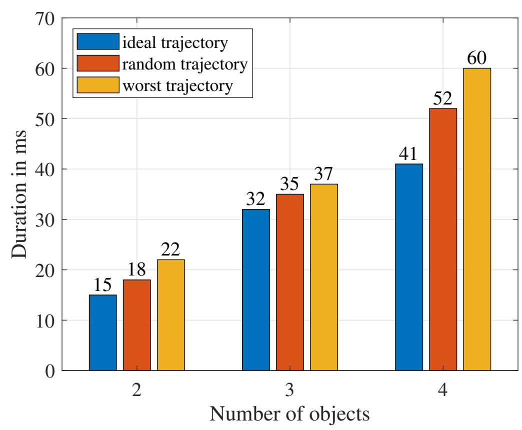


**Fig. 5.** Experimentally measured time required by the LRF and the FSM to measure the distance to multiple objects depending on the trajectory travelled by the FSM.

Fig. 5 shows the time needed by the LRF and the FSM to measure between 2 to 4 stationary objects comparing different trajectories taken by the FSM. The results indicate that a trajectory optimization already improves the performance when measuring the distance to two objects, as the path travelled by the FSM is reduced significantly compared to a random trajectory selection. The experimentally obtained bandwidth of the complete system, when applying trajectory optimization is 24 FPS for the measurement of one or two objects, 20 FPS for three objects and 14 FPS for four objects, when using a single LRF measurement per object. Fig. 6 shows an example of a multi-object distance measurement. The blurry image is the result of a small dichroic mirror (cf. Fig. 1a) not covering the aperture $L_1$ of the camera and therefore creating two optical paths for the visual light, which passes through and beside the dichroic mirror. As the dichroic mirror has a different refractive index than the surrounding air, the two optical paths distort the resulting image quality. The image quality can be improved either by using a large dichroic mirror that fills up the entire aperture or by reducing the size of the optical setup of $L_1$ and $L_2$ to fit the dichroic mirror. For the proof of concept the image quality is sufficient and does not reduce the performance of the used KCF tracker.

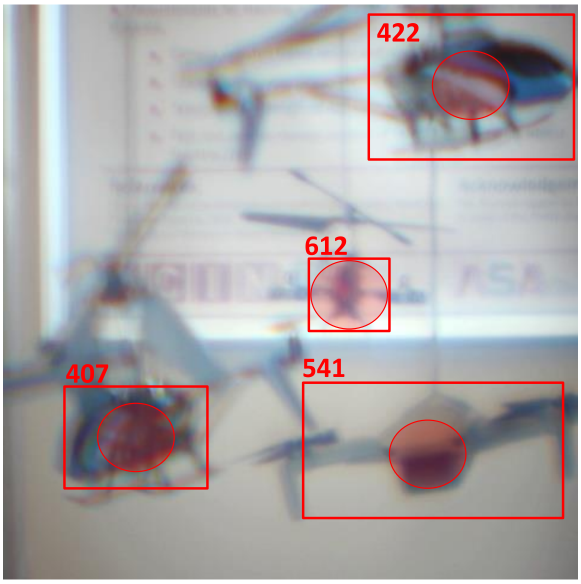


**Fig. 6.** Example of a multi-object distance measurement. The numbers on top of the bounding boxes indicates the distance to the objects in centimeter. The circle within the bounding boxes shows the size of the laser spot relative to the object size.

### C. Local scanning

A crucial consideration for the measurement of small and complex shaped objects like UAVs is the inherent possibility of missing the target. A reason for a laser pulse miss is inaccurate localization provided by the computer vision algorithm combined with inadequate laser beam divergence. For single LRF measurements, the best approach

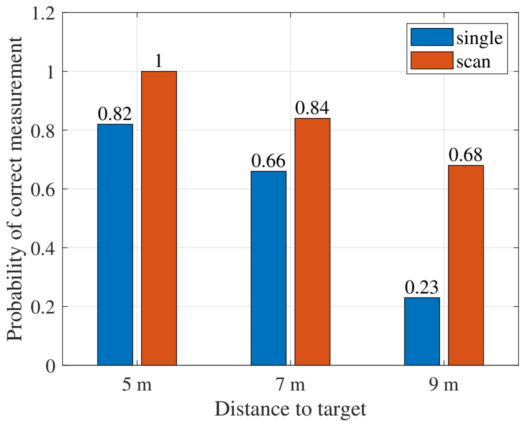


**Fig. 7.** Measured reliability of single LRF measurement compared to local scanning using 16 LRF measurements to obtain the distance. The bounding boxes are initialized with a random offset to the ideal ground truth bounding box. The random offset is in an interval between 1 and 0.5 regarding the intersection over union.

is to align the LRF with the bounding box center as depicted by the circles in Fig. 6. To reduce the number of miss measurements, the local scanning approach presented in Section 4 is used. For local scanning, a correct measurement is achieved, when the output of the clustering algorithm corresponds to the distance between UAV and the setup $\pm$ 0.1 m. Fig. 7 shows the results of comparing the single LRF measurement to the local scan, whereas a non ideal bounding box to object overlap is simulated. In object detection, an object is widely considered correctly detected, when the suggested bounding box overlaps with the ground truth bounding box by 50 % resulting in an intersection over union of 0.5 [45]. Therefore, for the evaluation, the tracker is initialized 50 times on a UAV with a random offset to the UAV center to simulate ideal and non-ideal tracker outputs. The offset between ground truth and initialized bounding box lies within 1 and 0.5 in terms of intersection over union and the reliability is calculated as the percentage of correct distance measurements. For the single measurement, a reduction in the measurement probability is observed for longer distances, which coincides with Fig. 3. If the bounding box is not accurately aligned with the target, not enough light is reflected to be detected by the LRF. The results clearly indicate an

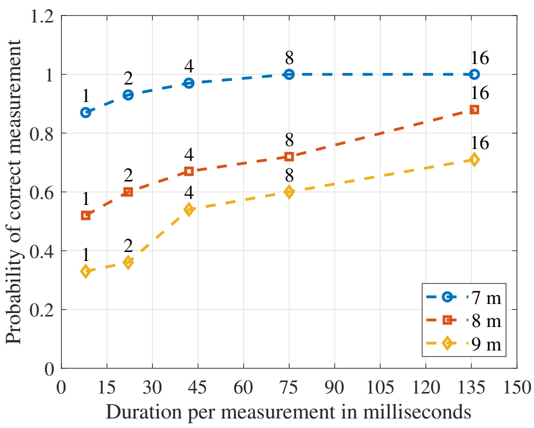


**Fig. 8.** Experimentally obtained probability of a correct distance inference, depending on the number of measurements performed by the local scanning. The markers denote 1, 2, 4, 8 and 16 measurements. The bounding box is initialized ideally on the object.

improved measurement reliability when using a local bounding box scan at the expense of a reduced system bandwidth. The impact on bandwidth is analysed in Fig. 8, where the probability of a correct measurement is plotted against the measurement duration. Different values for the duration are obtained by increasing the number of performed laser acquisitions from 1 to a maximum of 16 following a raster trajectory. Compared to Fig. 7 the one shot measurements score a higher probability, as the bounding box is initialized ideally on the UAV for this experiment. For longer distances, the probability of a correct measurement decreases, as the laser spot size is larger than the target object itself. By applying a local scanning measurement reliability can be increased.

The implemented small scale prototype system demonstrates real-time ranging of multiple UAVs enabling each second 14 distance measurements per object when measuring the distance to 4 objects. Furthermore, the probability to correctly measure the distance can be increased by introducing local scanning.

## 6. CONCLUSION

A scalable telescope based laser ranging system has been designed and developed that is capable to measure the distance to multiple UAVs using the positional information within a camera frame. The key concept is the combination of the optical paths of the visual light and the laser light, which allows fast laser to target alignment using an FSM. The laser beam is aligned based on information extracted by computer vision algorithms, making elaborate laser scanning of the whole FoV in search for a target redundant. This idea enables to perform a single LRF measurement to obtain the distance to a UAV, hence enabling multi UAV localization in real-time. With the proposed design and implemented prototype system a bandwidth of 14 Hz per object when measuring the distance to 4 objects and 20 Hz for 3 objects is achievable. The measurement reliability can be increased by introducing local scanning of the bounding box. Future work will focus on improving the measurement range, by incorporating a stronger laser with a smaller beam divergence and the integration of the system to a commercial telescope.

## 7. FUNDING

This publication has been funded by the Austrian defense research programme FORTE of the Federal Ministry of Agriculture, Regions and Tourism (BMLRT).

## 8. DISCLOSURES

The authors declate that there are no conflicts of interest related to this paper.

## 9. DATA AVAILABILITY

Data underlying the results presented in this paper are not publicly available at this time but may be obtained from the authors upon reasonable request.

## REFERENCES

1. C. F. Liew, D. DeLatte, N. Takeishi, and T. Yairi, "Recent Developments in Aerial Robotics: A Survey and Prototypes Overview," ArXiv **abs/1711.10085** (2017).
2. J. Serna, "Lufthansa jet and drone nearly collide near LAX," Los Angeles Times (2016). Accessed Feb 2022.
3. C. Phillips and C. Gaffey, "Most French Nuclear Plants 'Should Be Shut Down' Over Drone Threat," Newsweek Magazine (2015). Accessed Feb 2022.
4. A. Solodov, A. Williams, S. A. Hanaei, and B. Goddard, "Analyzing the threat of unmanned aerial vehicles (UAV) to nuclear facilities," Security Journal **31**, 305–324 (2017).
5. S. Dinan, "Mexican drug cartels using drones to smuggle heroin, meth, cocaine into U.S." The Washington Times (2015). Accessed Feb 2022.
6. "Charges over drone drug smuggling into prisons," BBC News (2018). Accessed Feb 2022.
7. H. Duan, D. Zhang, Y. Shi, and Y. Deng, "Close formation flight of swarm unmanned aerial vehicles via metric-distance brain storm optimization," Memetic Comput. **10**, 369–381 (2018).

Post-print version of the article: D. Ojdanic, B. Gräf, A. Sinn, H. W. Yoo, and G. Schitter, "Camera Guided Real-Time Laser Ranging for Multi-UAV Distance Measurement," *Applied Optics*, vol. 61, 2022. DOI: 10.1364/AO.470361

8. M. Gargalakos, "The role of unmanned aerial vehicles in military communications: application scenarios, current trends, and beyond," Journal of Defense Modeling and Simulation: Applications, Methodology, Technology. (2021).
9. S. Yang, H. Qin, X. Liang, and T. Gulliver, "An Improved Unauthorized Unmanned Aerial Vehicle Detection Algorithm Using Radiofrequency-Based Statistical Fingerprint Analysis," Sensors. **19**, 274 (2019).
10. W. Nie, Z.-C. Han, M. Zhou, L.-B. Xie, and Q. Jiang, "UAV detection and identification based on WiFi signal and RF fingerprint," IEEE Sensors J. **21**, 13540–13550 (2021).
11. V. Baron, S. Bouley, M. Muschinowski, J. Mars, and B. Nicolas, "Drone localization and identification using an acoustic array and supervised learning," in *Artificial Intelligence and Machine Learning in Defense Applications,* (11169F SPIE, 2019).
12. A. Sedunov, D. Haddad, H. Salloum, A. Sutin, N. Sedunov, and A. Yakubovskiy, "Stevens drone detection acoustic system and experiments in acoustics UAV tracking," in *2019 IEEE International Symposium on Technologies for Homeland Security (HST),* (IEEE, 2019).
13. S. Hu, G. H. Goldman, and C. C. Borel-Donohue, "Detection of unmanned aerial vehicles using a visible camera system," Appl. Opt. **56**, B214 (2017).
14. J. Farlik, M. Kratky, J. Casar, and V. Stary, "Multispectral Detection of Commercial Unmanned Aerial Vehicles," Sensors. **19**, 1517 (2019).
15. M. Rebert, "Prediction of micro-unmanned aerial vehicle flight behavior from two-dimensional intensity images," Opt. Eng. **58**, 1 (2019).
16. H. Jiang, L. Ding, Z. Sun, and R. Huang, "Unsupervised monocular depth perception: Focusing on moving objects," IEEE Sensors J. **21**, 27225–27237 (2021).
17. Z. Zhang, Y. Han, Y. Zhou, and M. Dai, "A novel absolute localization estimation of a target with monocular vision," Optik. **124**, 1218–1223 (2013).
18. A. Zaarane, I. Slimani, W. Al Okaishi, I. Atouf, and A. Hamdoun, "Distance measurement system for autonomous vehicles using stereo camera," Array. **5**, 100016 (2020).
19. A. D. De Quevedo, F. I. Urzaiz, J. G. Menoyo, and A. A. Lopez, "Drone Detection and RCS Measurements with Ubiquitous Radar," in *2018 International Conference on Radar (RADAR),* (2018), pp. 1–6.
20. T. Bosch, "Laser ranging: a critical review of usual techniques for distance measurement," Opt. Eng. **40**, 10 (2001).
21. X. Zhao, P. Sun, Z. Xu, H. Min, and H. Yu, "Fusion of 3D LiDAR and camera data for object detection in autonomous vehicle applications," IEEE Sensors J. **20**, 4901–4913 (2020).
22. M. Salhi and N. Boudriga, "Multi-Array Spherical LiDAR System for Drone Detection," in *2020 22nd International Conference on Transparent Optical Networks (ICTON),* (IEEE, 2020).
23. M. Hammer, M. Hebel, M. Laurenzis, and M. Arens, "LiDAR-based detection and tracking of small UAVs," in *Emerging Imaging and Sensing Technologies for Security and Defence III; and Unmanned Sensors, Systems, and Countermeasures,* vol. 10799 (2018), pp. 177 – 185.
24. G. Zhou, X. Zhou, J. Yang, Y. Tao, X. Nong, and O. Baysal, "Flash LiDAR sensor using fiber-coupled APDs," IEEE Sensors J. **15**, 4758–4768 (2015).
25. R. Horaud, M. Hansard, G. Evangelidis, and C. Ménier, "An overview of depth cameras and range scanners based on time-of-flight technologies," Mach. Vis. Appl. **27**, 1005–1020 (2016).
26. J. Martinez, A. Pequeno-Boter, A. Mandow, A. Garcia-Cerezo, and J. Morales, "Progress in Mini-Helicopter Tracking With a 3D Laser Range-Finder," IFAC Proc. Vol. **38**, 648–653 (2005).
27. A. Pawlikowska, R. Pilkington, K. Gordon, P. Hiskett, G. Buller, and R. Lamb, "Long-range 3D single-photon imaging LiDAR system," Proc. SPIE - Electro-Optical Remote. Sensing, Photonic Technol. Appl. VIII; Mil. Appl. Hyperspectral Imaging High Spatial Resolut. Sens. II **9250** (2014).
28. B. Kim, D. Khan, C. Bohak, W. Choi, H. Lee, and M. Kim, "V-RBNN Based Small Drone Detection in Augmented Datasets for 3D LADAR System," Sensors **18**, 3825 (2018).
29. A. G. Ledebuhr, J. F. Kordas, and I. T. Lewis, "HiRes camera and LiDAR ranging system for the Clementine mission," in *SPIE international symposium on aerospace/defense sensing and dual-use photonics,* (1995).
30. D. Joshi, D. Kumar, A. K. Maini, and R. C. Sharma, "Detection of biological warfare agents using ultra violet-laser induced fluorescence LIDAR," Spectrochimica Acta Part A: Mol. Biomol. Spectrosc. **112**, 446–456 (2013).
31. Z. Kong, T. Ma, Y. Cheng, Z. Zhang, Y. Li, K. Liu, and L. Mei, "Feasibility investigation of a monostatic imaging LiDAR with a parallel-placed image sensor for atmospheric remote sensing," J. Quant. Spectrosc. Radiat. Transf. **254**, 107212 (2020).
32. B.-H. Sheu, C.-C. Chiu, W.-T. Lu, C.-I. Huang, and W.-P. Chen, "Development of UAV tracing and coordinate detection method using a dual-axis rotary platform for an anti-UAV system," Appl. Sci. **9**, 2583 (2019).
33. A. Hommes, A. Shoykhetbrod, D. Noetel, S. Stanko, M. Laurenzis, S. Hengy, and F. Christnacher, "Detection of acoustic, electro-optical and RADAR signatures of small unmanned aerial vehicles," in *SPIE Proceedings,* (SPIE, 2016).
34. F. Christnacher, S. Hengy, M. Laurenzis, A. Matwyschuk, P. Naz, S. Schertzer, and G. Schmitt, "Optical and acoustical UAV detection," in *Electro-Optical Remote Sensing X,* (SPIE, 2016).
35. Aselsan, "IHTAR anti-drone system - datasheet," ASELSAN A.S., Ankara, Türkiye (2018).
36. D. Ojdanić, A. Sinn, C. Naveschnigg, and G. Schitter, "Feasibility Analysis of Optical UAV Detection Over Long Distances Using Robotic Telescopes ," IEEE Transactions on Aerosp. Electron. Syst. Submitted Mar. 2022.
37. R. D. Richmond and S. C. Cain, *Direct-Detection LADAR Systems* (SPIE Press, 2010).
38. J. Wojtanowski, M. Zygmunt, M. Kaszczuk, Z. Mierczyk, and M. Muzal, "Comparison of 905 nm and 1550 nm semiconductor laser rangefinders' performance deterioration due to adverse environmental conditions," Opto-Electronics Rev. **22** (2014).
39. S. Gundacker and A. Heering, "The silicon photomultiplier: fundamentals and applications of a modern solid-state photon detector," Phys. Medicine & Biol. **65**, 17TR01 (2020).
40. D. Bastos, P. P. Monteiro, A. S. Oliveira, and M. V. Drummond, "An overview of lidar requirements and techniques for autonomous driving," in *2021 Telecoms Conference (ConfTELE),* (IEEE, 2021), pp. 1–6.
41. H. Masoumi, S. S. Mohsen, and K. Zahra., "Identification and classification of plastic resins using near infrared reflectance spectroscopy," International Journal of Mechanical and Industrial Engineering. **6**, 213–220 (2012).
42. S. Zhu, H. Chen, M. Wang, X. Guo, Y. Lei, and G. Jin, "Plastic solid waste identification system based on near infrared spectroscopy in combination with support vector machine," Advanced Industrial and Engineering Polymer Research. **2**, 77–81 (2019).
43. "OpenCV Tracking API," Accessed: Feb. 2022.
44. Inframet, "LAS Test Station - inframet.com," Accessed: 2021-11-29.
45. R. Padilla, S. L. Netto, and E. A. B. da Silva, "A survey on performance metrics for object-detection algorithms," in *2020 International Conference on Systems, Signals and Image Processing (IWSSIP),* (IEEE, 2020).

Post-print version of the article: D. Ojdanic, B. Gräf, A. Sinn, H. W. Yoo, and G. Schitter, "Camera Guided Real-Time Laser Ranging for Multi-UAV Distance Measurement," *Applied Optics*, vol. 61, 2022. DOI: 10.1364/AO.470361